Desalination and Water Treatment
www.deswater.com

doi: 10.5004/dwt.2021.27321

228 (2021) 414–421
July

Photocatalytic degradation of 1:2 metal complex dye Acid blue 193 under solar light condition using ZnO nanoneedles and ZnO/bentonite nanocomposite synthesized via microwave irradiation

Nguyen Van Suc

Ho Chi Minh City University of Technology and Education, 01 Vo Van Ngan, Thu Duc, Ho Chi Minh City, Vietnam, email: sucnv@hcmute.du.vn

Received 11 December 2020; Accepted 12 April 2021

ABSTRACT

This paper describes a novel method for the preparation of ZnO nanoneedles and ZnO/bentonite nanocomposite with the assistance of a household microwave irradiation and their successful application for the photocatalytic degradation of 1:2 metal complex dye Acid blue 193 under solar energy. The products were analyzed by transmission electron microscopy (TEM), scanning electron microscopy (SEM), diffuse reflectance spectra and X-ray diffraction. The results confirm that synthesized ZnO nanoneedles are highly crystalline having a hexagonal wurtzite structure. TEM and SEM images show that wurtzite ZnO nanoneedles are well impregnated and homogeneously supported on the bentonite surface. The optical gap of ZnO nanoneedles was found to be 3.08 eV. The highest degradation efficiency of 1:2 metal complex dye Acid blue 193 was obtained at pH 8 for ZnO nanoneedles and ZnO/bentonite nanocomposite. In the kinetic study, the results for catalysts showed that the experimental data were fitted the pseudo-first-order model.

Keywords: ZnO nanoneedles; ZnO/bentonite nanocomposite; Heterogeneous catalysis; 1:2 metal complex dye Acid blue 193; Microwave irradiation

1. Introduction

Challenges associating with the effective treatment of wastewater from the textiles industry are well known, as it is a large source of water contamination [1]. Able to solve these challenges could lead to a tremendous positive impact on the development of the textile industry, especially in developing countries such as Vietnam where it is an important source of income and jobs. In general, from an economic view, a successful treatment method needs to be inexpensive, in both initial capital and ongoing operational cost.

One key in treat textile wastewater is how to remove effectively residue dyes. There are many methods available to solve this problem, each with its own advantages and disadvantages [2–4]. Among the known methods, advanced oxidation processes (AOPs) have been considered as one of the promising candidates because this method can efficiently oxidize a wide range of organic compounds found in water and wastewater [5–9]. In recent years, AOP based on heterogeneous catalysis using metal oxides as catalysts has attracted attention due to their acid–base and redox properties [10–16]. Among the various metal oxides, ZnO has been employed as a promising heterogeneous catalyst for various organic transformations, owing to its high activity, low cost, and environment-friendly. Further, ZnO has a diverse structural morphology, allowing its total surface areas to be fine-tuned by varying synthesis conditions to obtain different shapes which show significant difference from photocatalytic performances [17–20]. However, the disadvantages of the heterogeneous photocatalysis by using ZnO as well as other metal oxides in nanostructure are difficult to recover by sedimentation and filtration processes.

To overcome this difficulty, the catalysts are immobilized on the surface of some supporters such as activated carbon, bentonite, etc. This allows to enhance photocatalytic activity and to be recoverable and, potential, reusable with the operation and economic advantages [21–25].

For these reasons, the present study was carried out on synthetization of ZnO nanoneedles and immobilization of ZnO onto the purified bentonite surface via microwave irradiation. The study also performed to characterize and evaluate the photocatalytic activity of the products which are capable of decolorizing 1:2 metal complex dye Acid blue 193 under solar energy.

2. Experimental

2.1. Material and method

2.1.1. Dye solution preparation

Molecular structure and UV/vis spectra of 1:2 metal complex dye Acid blue 193 (MF: $C_{20}H_{13}CrN_2NaO_5S$; MW: 468.3785 g/mol) is shown in Figs. 1a and b, respectively. The stock of dye solution was prepared by dissolving 0.1 g of Acid blue 193 in 100 mL of distilled water. Working solutions at specific concentrations in the range from 5 to 20 mg/L were prepared by diluting the stock solution with distilled water.

2.1.2. Purification of raw bentonite

Raw bentonite was supplied by JSC Mineral & Building Materials LAM DONG, Vietnam. Raw bentonite was treated based on the method published procedure [26] with somewhat modification. 10 g of the raw bentonite were suspended in 500 mL distilled water and stirred magnetically for 24 h. The supernatant of the dispersion was separated by centrifugation at 4,500 rpm for 2 min to collect a fine suspension. This process is repeated 2–3 times. The final solid was collected after a second centrifugation step at 10,000 rpm, and then dried at 120°C for 6 h.

2.1.3. Preparation of ZnO nanoneedles and ZnO/bentonite nanocomposite

100 mL of 0.45 M solution of zinc acetate ($Zn(CH_3COO)_2{\cdot}2H_2O$) were added dropwise into a glasses beaker containing 100 mL of 0.9 M solution of sodium hydroxide under constant stirring. The mixture obtained was then irradiated in a household microwave oven at 800 W for 15 min. The solid formed was washed with distilled water and centrifugation at 10,000 rpm until the pH of the liquid phase was 6–6.5. The precipitates were dried at 150°C for 24 h. For the preparation of ZnO/bentonite nanocomposite, the procedure was performed as above, but the NaOH solution was thoroughly mixed with 10 g of purified bentonite.

2.1.4. Characterization of ZnO nanoneedles and ZnO/bentonite nanocomposite

The characteristics of ZnO nanoneedles and ZnO/bentonite nanocomposite were analyzed by transmission electron microscopy (TEM Model: JEOL JEM-1400, USA), scanning electron microscope (FT-SEM Model: Hitachi S-4800, Japan), and X-ray diffractometer (XRD Model: Bruker D8 Advance), respectively. The point of zero charge (pH_{zpc}) of ZnO nanoneedles and ZnO/bentonite nanocomposite was determined by acid/base titration method [27].

2.2. Photocatalytic activity test

All photocatalytic experiments were conducted on sunny days from 9 am to 3 pm in March and April of the year to minimize the variation of solar intensity. Specific amounts of ZnO nanoneedles (0.15–1.5 g/L) and ZnO/bentonite nanocomposite (0.5–3.5 g/L) were added into each of borosilicate glass conical flasks containing 200 mL of 1:2 metal complex dye Acid blue 193 at specific concentrations (5–20 mg/L). pH of the solutions was adjusted to desire values (4–10) using diluted H_2SO_4 and NaOH solutions. The reaction mixture was stirred with a magnetic stirrer and kept under sunlight for 180 min. Every 20 min, 5 mL of each solution was taken and centrifuged at 10,000 rpm to separate the catalyst. The concentration of the Acid blue 193 in the liquid phase was determined by UV-Vis spectrophotometry (Model UH415AD UV-Vis-NIR spectrophotometer).

3. Results and discussion

3.1. Characterization of the products

Figs. 2a and b show the TEM image of a ZnO nanoneedles crystal and ZnO/bentonite nanocomposite, respectively.

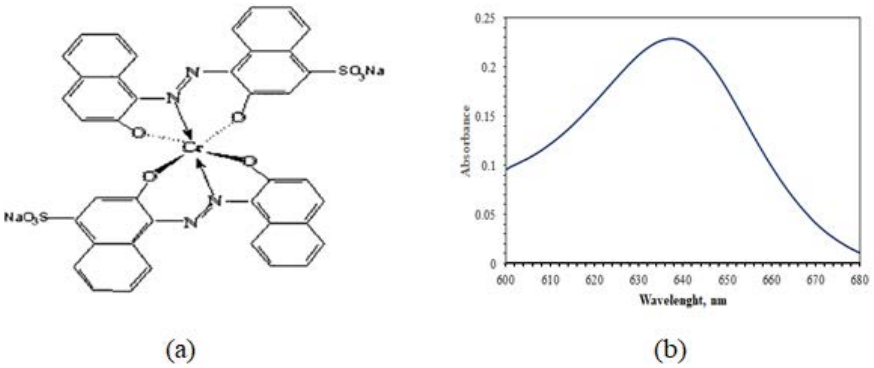

Fig. 1. (a) Structure and (b) UV/Vis spectra of 1:2 metal complex dye Acid blue 193.

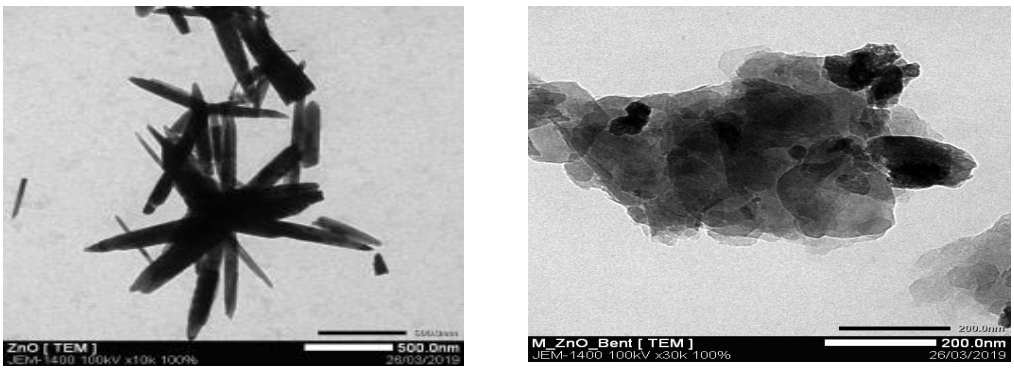

(a) (b)

Fig. 2. TEM image of (a) a single crystal of ZnO nanoneedles and (b) a single particle of ZnO/bentonite nanocomposite.

From Fig. 2a, it is clear that products are needle-shaped having straight sides and a wurtzite structure growing along the (001) direction, consisting of the result of X-ray diffraction (XRD) spectra of the product (Fig. 4c). The needles dimension is 100.0–118.3 nm in length, 16–19.2 nm in diameter at the main body, and 10.3–10.6 nm in diameter at the end of the needles. Fig. 2b shows ZnO nanoneedles dispersed on the surface of bentonite. Figs. 3a–c shows the surface morphology of ZnO nanoneedles, purified bentonite and ZnO/bentonite nanocomposite, respectively. The surface morphology of ZnO nanoneedles exhibits regulation shape and relative uniformity. The SEM images of ZnO nanoneedles, purified bentonite and ZnO/bentonite nanocomposite are presented in Figs. 3a–c. Fig. 3b shows that the purified bentonite has a pore structure, suitable for ZnO immobilization. As seen in Fig. 3c, the result is reflected in the wurtzite ZnO which is well impregnated and homogeneously supported on the purified bentonite surface.

The XRD patterns of raw bentonite, purified bentonite, ZnO nanoneedles and ZnO/bentonite nanocomposite are shown in Figs. 4a–d, respectively. Figs. 4a and b show an increase in the intensity of the characteristic peaks for smectite minerals of the purified bentonite (Fig. 4a) that could not observe in the raw bentonite (Fig. 4b). A peak at 15° in the XRD for the raw bentonite indicates that the sample from Lam Dong province was contaminated by kaolinite. However, this peak increased intensity in the purified bentonite showing the purification process did not help reduce this impurity. XRD patterns for the ZnO nanoneedles (Fig. 4c) and ZnO/bentonite nanocomposite (Fig. 4d) confirm that ZnO is a single-phase hexagonal nanocrystal structure. Fig. 4d shows mixed phases and contains peaks of ZnO and bentonite, indicating the successful impregnation of ZnO onto the purified bentonite surface. As a reference, all the diffraction peaks observed in the XRD spectra in Fig. 4c for the ZnO nanoneedles are either identical or close to JCPDE card No. 36–1451 [28,29].

Fig. 5 shows the UV-Vis diffuse reflectance spectra (DRS) of ZnO nanoneedles and ZnO/bentonite nanocomposite. From the results, it can be seen that the ZnO nanoneedles sample only has an absorbance at 393 nm corresponding to the ground excitonic state of ZnO. The presence of this peak also reflects the high crystalline nature of the nanoneedles with defects. However, ZnO/bentonite nanocomposite has a broader absorbance range in the visible light region ranging from 400 to 700 nm with a small and wide peak at 510 nm which confirms the formation of ZnO/bentonite in the heterostructures. This allows ZnO/bentonite nanocomposite to utilize both the ultraviolet and visible region of the solar light spectrum, leading to remarkably enhance its photocatalytic activity. Bandgap energy of ZnO nanoneedles prepared by our method was found to be 3.08 eV, using Tauc's relation [30] (plot not shown here). This value is smaller than those that have been reported [20].

3.2. Photocatalytic activity test for ZnO nanoneedles and ZnO/bentonite nanocomposite under solar energy

The photocatalytic activity of ZnO nanoneedles and ZnO/bentonite nanocomposite was evaluated via degradation of 1:2 metal complex dye Acid blue 193 (10 mg/L) at pH 5 and 0.5 g/L of catalysts under solar light irradiation condition. Fig. 6 shows that, for the blank test, without the presence of the catalysts, 1:2 metal complex dye Acid blue 193 concentration did not change after 200 min exposure to sunlight. In the presence of purified bentonite, approximately only 60%, probably due to the adsorption of dye onto the bentonite surface. However, in the presence of either ZnO nanoneedles or ZnO/bentonite nanocomposite, a significant reduction in the dye concentration was observed. The dye's degradation efficiency was found to be 76.0% for ZnO nanoneedles and 87.0% for ZnO/bentonite nanocomposite. It is interesting that the photoactivity of ZnO/bentonite nanocomposite is significantly higher than that of ZnO nanoneedles. This could be explanted that the adsorption of dye on bentonite surface of ZnO/bentonite nanocomposite surface can cause a synergistic effect that enhances the removal efficiency of 1:2 metal complex dye Acid blue 193 [31].

3.3. Effect of pH

pH of the solution typically has an important role in the process as it impacts the surface charge of the catalyst surface and the charge of pollutant ions existing in an aqueous solution [32,33]. The pHzpc of ZnO nanoneedles and ZnO/bentonite nanocomposite were found to be 8.9 and 9.5, respectively (the plots not shown here). At low pH, 1:2 metal complex dye Acid blue 193 mainly exits in anion

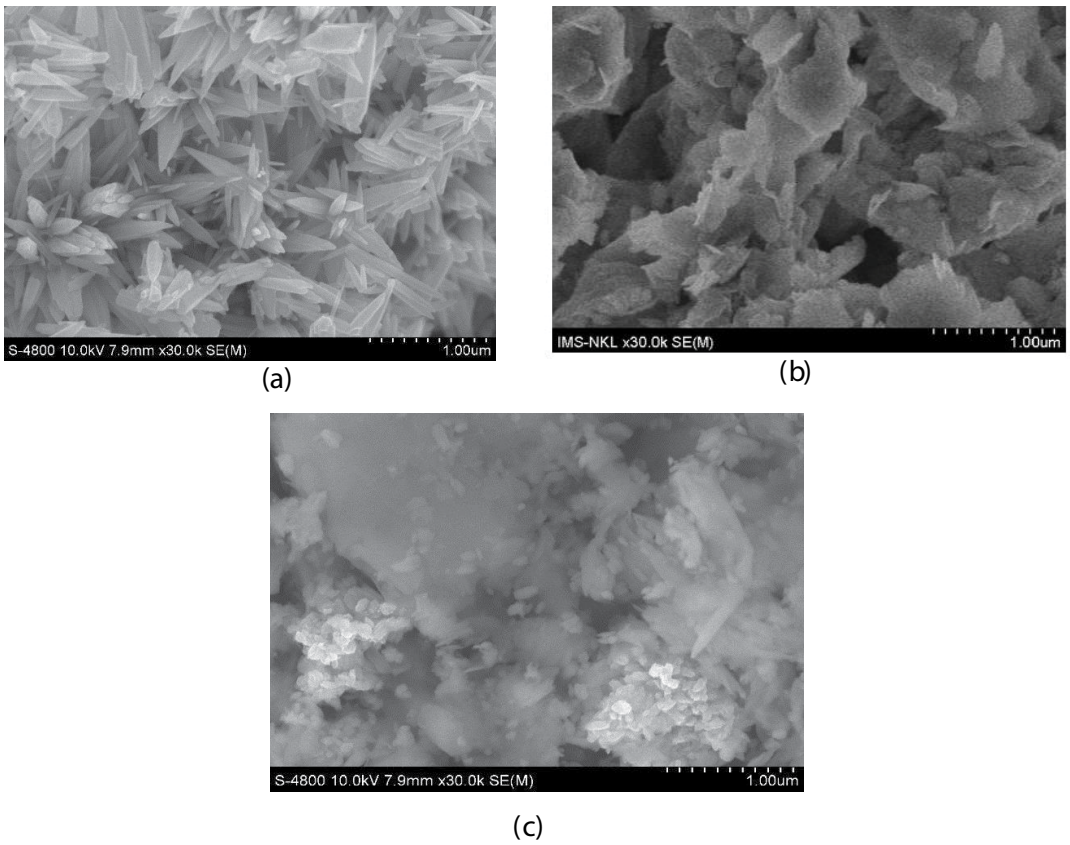

Fig. 3. The surface morphology of (a) ZnO nanoneedles, (b) purified bentonite and (c) ZnO/bentonite nanocomposite.

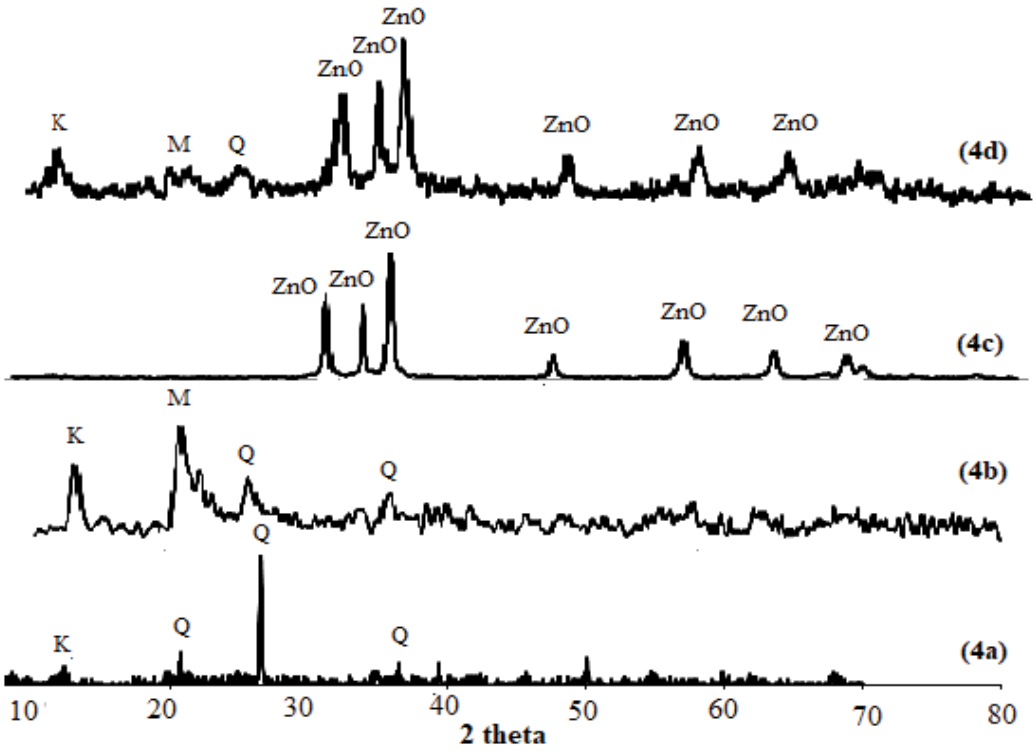

Fig. 4. XRD spectra of (a) raw bentonite, (b) purified bentonite, (c) ZnO nanoneedles and (d) ZnO/bentonite nanocomposite; (Q: quartz; K: kaolinite; M: montmorillonite).

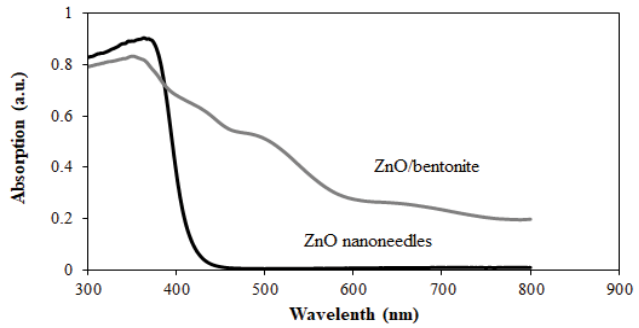

Fig. 5. UV-Vis DRS of ZnO nanoneedles and ZnO/bentonite nanocomposite.

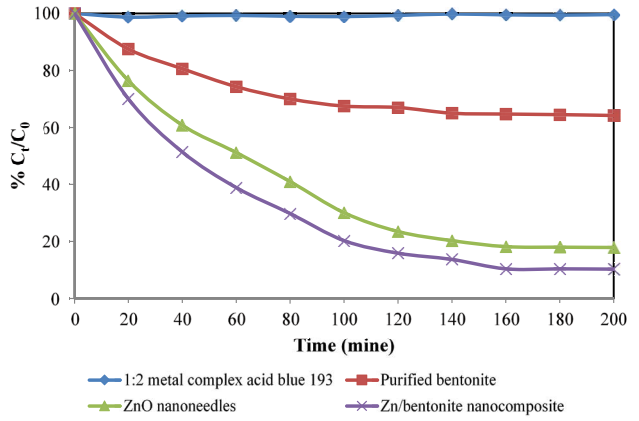

Fig. 6. Photocatalytic activity of ZnO nanoneedles and ZnO/bentonite nanocomposite for degradation of 1:2 metal complex dye Acid blue 193 (10 mg/L) at pH 8 and 0.5 g/L of catalysts under solar light irradiation condition.

species that could be attracted to the positively charged surface of catalysts due to electrostatic interaction. Thus, the adsorption in this pH range is an important factor in the photocatalytic process, especially for the hetero-system ZnO/bentonite. However, at high pH environment, the adsorption can be reduced but more hydroxyl radical (•OH) form from hydroxide ions, leading to an increase in the degradation rate according to the following reactions [34]:

$$ZnO + h\nu \rightarrow (ZnO)e^{-}_{CB} + h^{+}_{VB} \quad (1)$$

$$h^{+}_{VB} + dye \rightarrow dye^{\bullet+} \quad (2)$$

$$h^{+}_{VB} + OH \rightarrow {}^{\bullet}OH \quad (3)$$

To elucidate the pH effect, experiments were conducted in a pH range from 4 to 10, at constant 1:2 metal complex dye Acid blue 193 (10 mg/L) and catalyst dose of 0.5 g/L of catalysts. The results are presented in Figs. 7a and b show that at pH 8, the degradation efficiencies of 1:2 metal complex dye Acid blue 193 reaches more than 90% for ZnO nanoneedles (Fig. 7a) and 94.0% for ZnO/bentonite nanocomposite (Fig. 7b) after 180 min of exposure to sunlight.

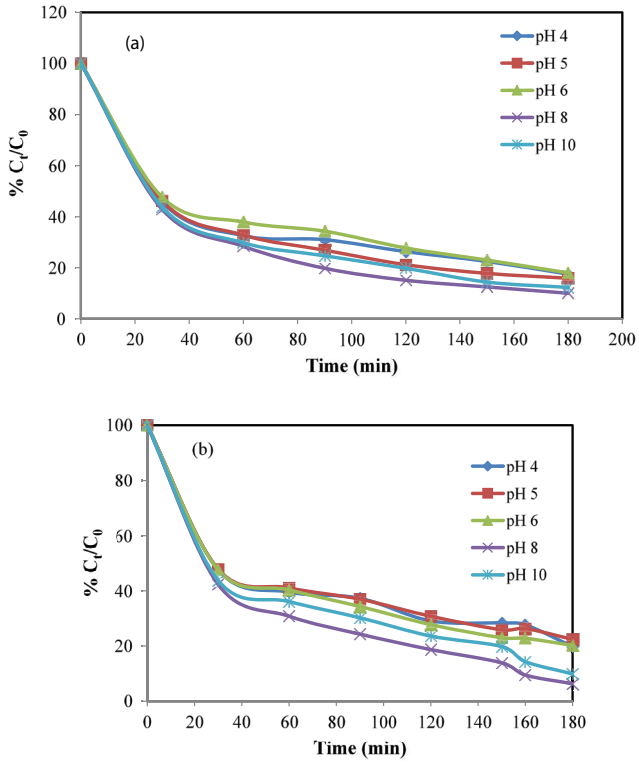

Fig. 7. Effect of pH on the photocatalytic degradation rate of 1:2 metal complex dye Acid blue 193, (a) for ZnO nanoneedles and (b) for ZnO/bentonite nanocomposite.

3.4. Effect of initial 1:2 metal complex Acid blue 193 concentrations

Figs. 8a and b show the degradation rate in different initial concentrations of 1:2 metal complex dye Acid blue 193 (5, 10, 15 and 20 mg/L) at pH 8 for ZnO nanoneedles, and ZnO/bentonite nanocomposite, respectively. From the results obtained, it could be seen that the degradation rate was inversely proportional with the increase in initial concentrations of 1:2 metal complex dye Acid blue 193 for both catalysts. Two reasons that lead to an undesirable consequence are (i) when the concentration of the dye in solution is high, dye molecules are adsorbed on the catalyst's surface resulting in the active sites on the catalyst surface being obscured, reducing the amount of free active radicals; (ii) the light penetration is strongly reduced as high initial concentration of dye increases. This leads to very few photons can reach to the catalyst surface [35].

3.5. Effect of catalytic dose

Figs. 9a and b show the variation of the degradation rate of 1:2 metal complex dye Acid blue 193 (10 mg/L) using different amount of ZnO/bentonite nanocomposite and ZnO nanoneedles. pH of the reaction solutions was adjusted to 8 for both ZnO/bentonite nanocomposite and ZnO nanoneedles. The degradation rate increased within the range 0.15–1.5 g/L of ZnO nanoneedles s (Fig. 9a), and, slightly wider, from 0.5 to 3.5 g/L of ZnO/bentonite nanocomposite

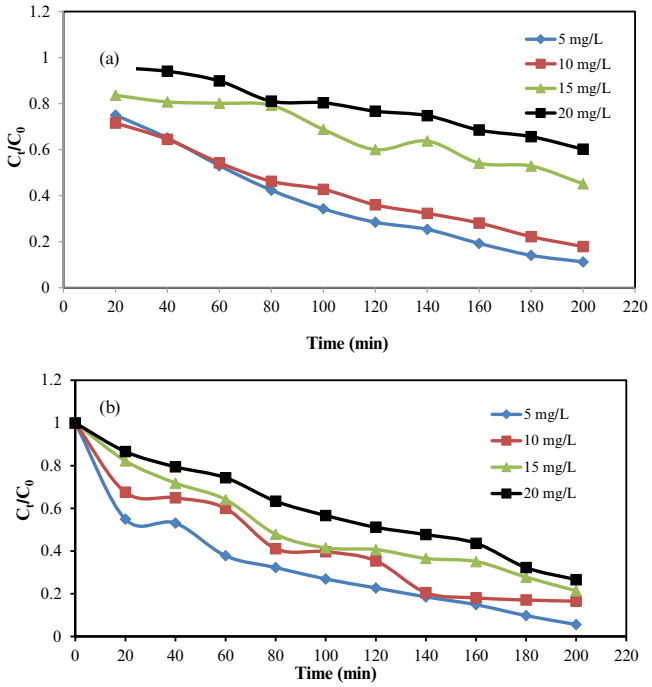

Fig. 8. Effect of initial concentrations of 1:2 metal complex dye Acid blue 193 on the photocatalytic degradation rate at pH 8, 0.5 g/L of catalysts, (a) ZnO nanoneedles and (b) ZnO/bentonite nanocomposite.

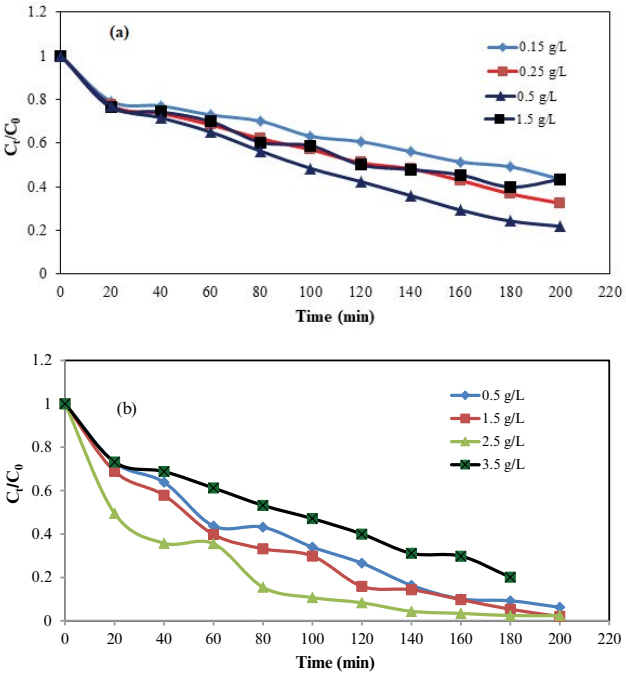

Fig. 9. Effect of catalytic dose on the photocatalytic degradation rate of 1:2 metal complex dye Acid blue 193 (10 mg/L), at pH 8, (a) for ZnO nanoneedles and (b) for ZnO/bentonite nanocomposite.

(Fig. 9b). The photocatalytic degradation rate was reduced when the catalytic amount used outside of those ranges (lower than 0.5 g/L for ZnO nanoneedles or higher than 3.5 g/L for ZnO/bentonite nanocomposite). This indicates that too much catalyst loading could reduce the depth of light penetration into the solution [36].

3.6. Photodegradation kinetics

It was observed that the photodegradation rate was inversed proportional with the increase in initial concentrations of 1:2 metal complex dye Acid blue 193 for both catalysts and catalysts dose for both catalysts (Figs. 8a and b, Figs. 9a and b). In order to evaluate the experimental data and describe the photocatalytic process, the pseudo-first-order and the pseudo-second-order kinetic models are used to evaluate the experimental data. The integrated forms of the two kinetic models are described as Eqs. (4) and (5) [37]:

The pseudo-first-order model:

$$\ln\left(\frac{C_0}{C_t}\right) = k_{obs1}t \tag{4}$$

The pseudo-second-order model:

$$\frac{1}{C_t} = \frac{1}{C_0} - k_{obs2}t \tag{5}$$

where C_0 and C_t are the concentrations of 1:2 metal complex Acid blue 193 at an initial time and time t; k_{obs1} (1/min) and k_{obs2} (L/mg min) are degradation reaction rate constants of

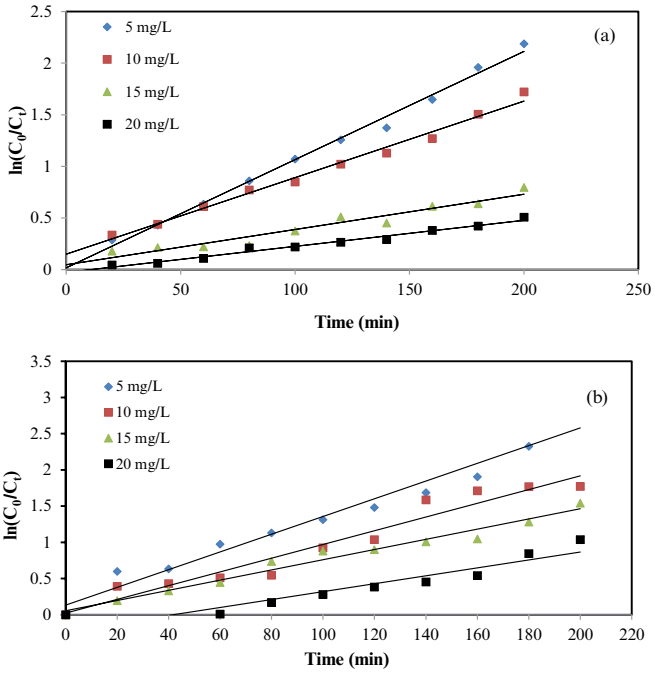

Fig. 10. The plots of $\ln(C_0/C_t)$ vs. time for the photocatalytic degradation processes of 1:2 metal complex dye acid blue, (a) ZnO nanoneedles and (b) ZnO/bentonite nanocomposite.

the pseudo-first-order and the pseudo-second-order models, respectively.

The k_{obs1} and k_{obs2} can be determined by plotting $\ln(C_0/C_t)$ or $1/C_t$ vs. t (Fig. 10a for data from tests using ZnO

Table 1
Calculated parameters of pseudo-first-order and pseudo-second-order models for the degradation rate of 1:2 metal Acid blue 193 by ZnO nanoneedles and ZnO/bentonite nanocomposite

Initial concentration (mg/L)	Pseudo-first-order				Pseudo-second-order			
	ZnO nanoneedles		ZnO/bentonite nanocomposite		ZnO nanoneedles		ZnO/bentonite nanocomposite	
	k_{obs1} (1/min)	R^2	k_{obs1} (1/min)	R^2	k_{obs2} (L/mg min^{-1})	R^2	k_{obs2} (L/mg min^{-1})	R^2
5	0.010	0.994	0.012	0.954	0.007	0.929	0.014	0.731
10	0.008	0.987	0.009	0.933	0.002	0.914	0.003	0.006
15	0.004	0.949	0.008	0.937	0.0004	0.908	0.011	0.912
20	0.002	0.981	0.006	0.964	0.0002	0.965	0.0006	0.879

nanoneedles and Fig. 10b for ZnO/bentonite nanocomposite). Plots of $1/C_t$ vs. t for both catalysts not shown here. The calculated parameters for both kinetic models are given in Table 1. This evaluation shows that the pseudo-first-order model is the better fit to describe the photodegradation data of 1:2 metal complex dye Acid blue 193 using both catalysts.

4. Conclusion

ZnO nanoneedles and ZnO/bentonite nanocomposite were successfully synthesized with the assistance of a household microwave irradiation. The products were characterized by TEM, SEM, XRD and DRS methods. The obtained results confirm that ZnO nanoneedles are hexagonal wurtzite structures and homogeneously supported on the purified bentonite surface. Both ZnO nanoneedles and ZnO/bentonite nanocomposite exhibit high photocatalytic activity via the decolorization of 1:2 metal complex dye Acid blue 193. The experimental data were found to be fitted the pseudo-first-order kinetic model for both catalysts.

Acknowledgments

The authors are thankful to Ms. Nguyen Thi Thanh Tuyen and Ms. Huynh Thi An Nhien for their technical assistance.

References

[1] S. Madhav, A. Ahamad, P. Singh, P.K. Mishra, A review of textile industry: wet processing, environmental impacts, and effluent treatment methods, Environ. Qual. Manage., 27 (2018) 31–41.
[2] K. Singh, S. Arora, Removal of synthetic textile dyes from wastewaters: a critical review on present treatment technologies, J. Crit. Rev. Environ. Sci. Technol., 41 (2011) 807–879.
[3] C. Ahmed Basha, K.V. Selvakumar, H.J. Prabhu, P. Sivashanmugam, C.W. Lee, Degradation studies for textile reactive dye by combined electrochemical, microbial and photocatalytic methods, Sep. Purif. Technol., 79 (2011) 303–309.
[4] S. Selvakumar, R. Manivasagan, K. Chinnappan, Biodegradation and decolourization of textile dye wastewater using *Ganoderma lucidum*, 3 Biotech., 3 (2013) 71–79.
[5] A. Al-Kdasi, A. Idris, C. Saed, C.T. Guan, Treatment of textile wastewater by advanced oxidation processes – a review, Global Nest: Int. J., 6 (2004) 222–230.
[6] M.A. Rauf, S.S. Ashraf, Chapter 9 – Application of Advanced Oxidation Processes (AOP) to Dye Degradation – An Overview, A.R. Lang, Ed., Dyes and Pigments: New Research ISBN 978-1-60692-027-5, Nova Science Publishers, Inc., 2009, pp. 259–307.
[7] A. El Nemr, M.A. Hassaan, F.F. Madkour, Advanced oxidation process (AOP) for detoxification of acid red 17 dye solution and degradation mechanism, Environ. Process., 5 (2018) 95–113.
[8] A. Zuorro, R. Lavecchia, Evaluation of UV/H_2O_2 advanced oxidation process (AOP) for the degradation of diazo dye reactive green 19 in aqueous solution, Desal. Water Treat., 52 (2013) 1571–1577.
[9] M.A. Hassaan, A. El Nemr, F.F. Madkour, Testing the advanced oxidation processes on the degradation of direct blue 86 dye in wastewater, Egypt. J. Aquat. Res., 43 (2017) 11–19.
[10] A.O. Ibhadon, P. Fitzpatrick, Heterogeneous photocatalysis: recent advances and applications, Catalysts, 3 (2013) 189–218.
[11] M.G. Alalm, A. Tawfik, S. Ookawara, Enhancement of photocatalytic activity of TiO_2 by immobilization on activated carbon for degradation of pharmaceuticals, J. Environ. Chem. Eng., 4 (2016) 1929–1937.
[12] P. Muthirulan, M. Meenakshisundararam, N. Kannan, Beneficial role of ZnO photocatalyst supported with porous activated carbon for the mineralization of alizarin cyanin green dye in aqueous solution, J. Adv. Res., 4 (2013) 479–484.
[13] Z.-A. Mirian, A. Nezamzadeh-Ejhieh, Removal of phenol content of an industrial wastewater via a heterogeneous photodegradation process using supported FeO onto nanoparticles of Iranian clinoptilolite, Desal. Water Treat., 57 (2016) 16483–16494.
[14] H.J. Cheng, L.Z. Wang, Nanostructure sensitization of transition metal oxides for visible-light photocatalysis, Beilstein J. Nanotechnol., 5 (2014) 696–710.
[15] A.K. Arora, V.S. Jaswal, K. Singh, R. Singh, Applications of metal/mixed metal oxides as photocatalyst: a review, Orient. J. Chem., 32 (2016) 2035–2042.
[16] J.C. Védrine, Heterogeneous catalysis on metal oxides, Catalysts, 7 (2017) 2–25.
[17] G. Kumar, R. Kumar, S.W. Hwang, A. Umar, Photocalytic degradation of direct red-23 dye with ZnO nanoparticles, J. Nanosci. Nanotechnol., 14 (2014) 7161–7166.
[18] S. Charkrabarti, B.K. Dutta, Photocatalytic degradation of model textile dyes in wastewater using ZnO as semiconductor catalyst, J. Hazard. Mater., 112 (2004) 269–278.
[19] K. Byrappa, A.K. Subramani, S. Ananda, K.M. Lokanatha Rai, R. Dinesh, M. Yoshimura, Photocatalytic degradation of rhodamine B dye using hydrothermally synthesized ZnO, Bull. Mater. Sci., 29 (2006) 433–438.
[20] P.K. Samanta, Weak quantum confinement in ZnO nanorods: a one dimensional potential well approach, Opt. Photonics Lett., 4 (2011) 35–45.
[21] M.A.M. Adnan, N.M. Julkapli, S.B.A. Hamid, Review on ZnO hybrid photocatalyst: impact on photocatalytic activities of water pollutant degradation, Rev. Inorg. Chem., 36 (2016) 77–104.
[22] A. Nezamzadesh-Ejhieh, S. Khosandi, Photocatalytic degradation of 4-nitrophenol with ZnO supported nanoclinoptililite zeolite, J. Ind. Eng. Chem., 20 (2014) 937–946.
[23] D. Rakhmawaty, S. Ishmayana, A.R. Noviyanti, Preparation of ZnO/SiO_2 composite using isolated from rice husk, Res. J. Chem. Environ., 22 (2018) 236–239.

[24] K. Rasool, G.K. Nasrallah, N. Younes, R.P. Pandey, P.A. Rasheed, K.A. Mahmoud, "Green" ZnO-interlinked chitosan nanoparticles for the efficient inhibition of sulfate-reducing bacteria in inject seawater, ACS Sustainable Chem. Eng., 6 (2018) 2896–3906.
[25] H.S. Zakria, M.H.D. Othman, R. Kamaludin, S.H.S.A. Kadir, T.A. Kurniawan, A. Jilani, Immobilization techniques of a photocatalyst into and onto a polymer membrane for photocatalytic activity, RCS Adv., 11 (2021) 6985–7014
[26] Z. Gong, L. Liao, G. Lv, X. Wang, A simple method for physical purification of bentonite, Appl. Clay Sci., 119 (2016) 292–300.
[27] N.V. Suc, D.T.K. Chi, Removal of rhodamine B from aqueous solution via adsorption onto microwave-activated rice husk ash, J. Dispersion Sci. Technol., 38 (2017) 216–222.
[28] T.M. Elmorsi, M.F. Bakr, M. Elsayed, Enhancing the removal of methylene blue by a modified ZnO nanoparticles, kinetics and equilibrium studies, Can. J. Chem., 95 (2017) 590–600.
[29] A. Pimentel, D. Nunes, P. Duarte, J. Rodrigues, F.M. Costa, T. Monterio, R. Martins, E. Fortunato, Synthesis of long ZnO nanorods under microwave irradiation or conventional heating, J. Phys. Chem., 118 (2014) 14629–14639.
[30] B.D. Viezbicke, S. Patel, B.E. Davis, D.P. Birnie, Evaluation of the Tauc method for optical absorption edge determination: ZnO thin film as a model system, Phys. Status Solidi B., 252 (2015) 1700–1710.
[31] S. Natarajian, H.C. Bajaj, R.J. Tayade, Recent advances based on the synergetic effect of adsorption for removal of dyes from waste water using photocatalytic process, J. Environ. Sci., 65 (2018) 201–222.
[32] N. Kamarulzaman, M.F. Kasim, R. Rusdi, Band gap narrowing and widening of ZnO nanostructures and dope materials, Nanoscale Res. Lett., 10 (2015) 1–12.
[33] L.A. Ghule, A.A. Patil, K.B. Sapnar, S.D. Dhole, K.M. Garadkar, Photocatalytic degradation of methyl orange using ZnO nanorods, Toxicol. Environ. Chem., 93 (2011) 623–634.
[34] A.F. Alkaim, A.M. Aljeboree, N.A. Alrazaq, S.J. Baqir, F.H. Hussein, A.J. Lilo, Effect of pH on adsorption and photocatalytic degradation efficiency of different catalysts on removal of methyl blue, Asian J. Chem., 26 (2014) 8445–8448.
[35] R. Kumar, G. Kumar, A. Umar, ZnO nano-mushrooms for photocatalytic degradation of methyl orange, Mater. Lett., 97 (2013) 100–103.
[36] M.S. Nasrollahzadeh, M. Hadavifar, S.S. Ghasemi, M.A. Chamjangali, Synthesis of ZnO nanostructure using activated carbon for photocatalytic degradation of methyl orange from aqueous solutions, Appl. Water Sci., 8 (2018) 104, doi: 10.1007/s13201-018-0750-6.
[37] M. Irani, T. Mohammadi, S. Mohebbi, Photocatalytic degradation of methylene blue with ZnO nanoparticles; a joint experimental and theoretical study, J. Mex. Chem. Soc., 60 (2016) 218–225.